J. Shao, Q. Zhou, D. Ye, F. Bernelli Zazzera, Z. Sun
Feasibility Analysis and Synchronization Control for Underactuated Spacecraft Formation Hovering
IEEE Transactions on Control Systems Technology, published online 18/07/2023
doi:10.1109/TCST.2023.3293989

Feasibility Analysis and Synchronization Control for Underactuated Spacecraft Formation Hovering

Jiang Shao, Qingrui Zhou, Dong Ye, Franco Bernelli-Zazzera, and Zhaowei Sun

***Abstract*—This paper develops a synchronization control scheme for underactuated spacecraft formation hovering in the case without along-track thrust. The feasible sets of initial positions for this underactuated case are derived based on the nonlinear and linear relative orbital dynamics. Then, a non-preset parameter underactuated controller is designed to deal with the unmatched disturbances caused by the loss of along-track control. Moreover, a synchronization item is added to the above controller to synchronize the hovering motion between the follower spacecraft. The Lyapunov-based analysis indicates that the minimum nonzero eigenvalue of the Laplace matrix corresponding to the synchronization item determines the stable hovering accuracy of the system states. Numerical simulations also demonstrate the validity of the presented underactuated synchronization controller.**

***Index Terms*—Feasible sets, stable hovering accuracy, synchronization control, underactuated spacecraft formation hovering, unmatched disturbances.**

I. Introduction

Spacecraft formation hovering is defined as the follower keeping a constant position relative to the leader, thus being in an equilibrium state [1, 2]. Compared to formation reconfiguration [3, 4] and satellite constellation [5], such a hovering strategy is more convenient for space exploration and provides higher resolution observation and measurement [6, 7]. Most of the existing control schemes presented for formation hovering, whether open- [8] or closed-loop ones [9], are based on the fully-actuated dynamics [10]. However, the fully-actuated controllers are not suitable for the underactuated case because the degrees of freedom of the input provided by the controller is 2, which is less than the degrees of freedom of the system states. Indeed, the system is still controllable in the absence of radial thrust, while the uncontrollable case without along-track thrust is more challenging. The feasibility of relative orbital control in both underactuated cases has already been researched for formation flying [11, 12]. Godard found an uncontrollable eigenvalue in the linearized relative dynamics and thus demonstrated the feasibility of underactuated formation flying [11].

Current works on the feasibility of underactuated formation hovering mainly concentrate on discussing the desired hovering positions [13–15] but do not analyze the initial motion states. In [13], Huang noted that due to the lack of thrust in a certain direction, the follower cannot hover in an arbitrary position relative to the leader. Hence, he derived the feasible set of desired hovering positions for either underactuated case. Then, he stated that the feasible desired positions are related to the loss of thrust and the input saturation constraint of the thrust in every direction [14]. According to the aforementioned feasible desired positions, we know where the underactuated spacecraft could hover. In contrast, it is also valuable to investigate the feasible set of initial positions, which indicates where the follower comes from, perhaps a specific hovering position or a natural formation.

In consideration of the existing underactuated formation controllers [12–15], one of the major challenges is that partial control parameters are preset. Generally, the initial values of the control parameters are set based on theoretical analysis and engineering experience, then these parameters are adjusted through many numerical simulations until the relevant dynamic indicators of the system satisfy the project requirements [16]. Such an operation that presets partial parameters not only restricts the coupling relationship between the error states in the controller but also predetermines the stable hovering accuracy of the system states, thus affecting the robustness of the designed controller [17, 18]. In addition, the expression of the unmatched disturbance is also determined by the prescribed control parameters. In view of these facts, this paper devotes to developing an underactuated controller that does not depend on preset control parameters. Unmatched disturbance is also a concern because traditional sliding mode control may lose invariance in the presence of unmatched disturbance, resulting in a system behavior in the sliding mode that will be governed by sliding surface and unmatched disturbance [11]. In the underactuated formation flying problem, since the loss of control input in the radial or along-track direction, the original disturbance no longer enters the system through the original channel but from one channel. Both matched disturbances are not simply added but multiplied by some matrices and added. In other words, the induced norms of these matrices will magnify the original disturbances by a certain multiple and then affect the control accuracy of the system.

This work was supported in part by the National Natural Science Foundation of China under Grants U21B2008, 62073102, 62203145, and 62173330, in part by the National Key Research and Development Program of China under Grant 2021YFC2202900, in part by Civil Aerospace Research Project of China under Grant D030312, and in part by China Scholarship Council. *(Corresponding author: Dong Ye)*

J. Shao is with the Research Center of Satellite Technology, Harbin Institute of Technology, Harbin 150001, China. He is an Official Joint Ph.D. Student, Qian Xuesen Laboratory of Space Technology, China Academy of Space Technology, 104 Youyi Road, Beijing. He is also a Visiting Student, Department of Aerospace Science and Technology, Politecnico di Milano, Milano, 20156, Italy. Q. Zhou is with the Qian Xuesen Laboratory of Space Technology, China Academy of Space Technology, Beijing 100094, China. D. Ye, and Z. Sun are with the Research Center of Satellite Technology, Harbin Institute of Technology, Harbin 150001, China. F. Bernelli-Zazzera is with the Department of Aerospace Science and Technology, Politecnico di Milano, Milano, 20156, Italy. (e-mail: shaojiang0805@hit.edu.cn; zhouqingrui@spacechina.com; yed@hit.edu.cn; franco.bernelli@polimi.it; sunzhaowei@hit.edu.cn).

Huang mentioned this challenge and introduced a disturbance observer to estimate the real value of unmatched disturbance [13]. Notably, the strong assumption that the observation error is zero and the conclusion that the stable hovering accuracy is zero are not suitable for practical engineering applications.

Synchronization control is also an issue for formation flying that has attracted wide attention [19, 20]. Synchronization motions between robots can remain the relative state relationship to maintain the specified, and perhaps time-varying, configuration. Although various synchronization controllers have been designed for formation control, most are developed for the fully-actuated system [19–21]. Moreover, in spite of the synchronization control does not affect the convergence of the system [19, 22]. It should be noted that the relative position, relative velocity, and control inputs of the system are slightly changed after adding the synchronization control item. Consequently, exploring the internal mechanism of such changes is meaningful, contributing to understanding synchronization control further.

Inspired by the above discussions, the main contributions of this study could be summarized into three aspects:

1) Compared to the previous feasible position analyses for underactuated formation hovering [13, 14], we derive the feasible set of initial positions via nonlinear and linear relative orbital dynamics and analyze the relationship between the initial and desired positions.
2) In comparison with the existing underactuated control approaches [12–15], a novel non-preset parameter underactuated controller is proposed to deal with the unmatched disturbances caused by the loss of along-track control, thereby improving the robustness of the closed-loop system.
3) Furthermore, a synchronization controller is designed to synchronize the follower's hovering motion with that of the neighboring followers. To our knowledge, this is the first time to prove the finite-time convergence of synchronization control. A new conclusion is obtained: the Laplace matrix's minimum nonzero eigenvalue determines the system states' stable hovering accuracy.

The rest of this brief is organized as follows. Section II derives the feasible set of initial positions. Section III describes the underactuated control scheme, including controller design and convergence analysis. Numerical simulations are presented in Section IV. Conclusions are driven in Section V.

Notations: $\mathbb{R}$ denotes the set of real numbers and ∂ is used to indicate the partial derivative. The Euclidean norm of a vector or a matrix is indicated by $\|\cdot\|$. $\lambda_{\min}(\cdot)$ is the minimum nonzero eigenvalue of a matrix. Set $\boldsymbol{v} = [v_1, v_2, ..., v_n]^{\mathrm{T}} \in \mathbb{R}$ as a vector, we define $\mathrm{sig}^{\gamma}(\boldsymbol{v}) = [|v_1|^{\gamma}\mathrm{sgn}(v),\ |v_2|^{\gamma}\mathrm{sgn}(v_2),\ ...\ ,\ |v_n|^{\gamma}\mathrm{sgn}(v_n)]^{\mathrm{T}}$ and $\boldsymbol{v}^{q/p} = [v_1^{q/p},\ v_2^{q/p},\ ...\ ,\ v_n^{q/p}]^{\mathrm{T}}$, where $0 < \gamma < 1$ is a constant, q and p are odd integers, and $\mathrm{sgn}(\cdot)$ is the sign function. $\mathrm{diag}(v_1, v_2, ..., v_n)$ is denoted as a diagonal matrix.

II. Dynamics and feasibility analysis

A. Dynamical Model

Suppose the leader flies in a circular Earth orbit and some followers hover nearby. We describe the dynamics of formation hovering in the local-vertical-local-horizontal (LVLH) frame, where x-axis is along the geocentric position vector of the leader, z-axis is positive in the direction of the orbital angular momentum vector, and y-axis is determined by the right-handed Cartesian frame. By denoting the position and velocity vectors of the ith $(i = 1, 2, ..., n)$ follower relative to the leader as $\boldsymbol{\rho}_i = [x_i\ y_i\ z_i]^{\mathrm{T}}$ and $\boldsymbol{v}_i = [\dot{x}_i\ \dot{y}_i\ \dot{z}_i]^{\mathrm{T}}$, the underactuated dynamical equation is described as follows.

$$\ddot{\boldsymbol{\rho}}_i = \boldsymbol{F}(\boldsymbol{\rho}_i, \boldsymbol{v}_i) + \tilde{\boldsymbol{U}}_i, \tag{1}$$

where $\boldsymbol{F} = [f_x\ f_y\ f_z]^{\mathrm{T}} = [2\dot{u}_l\dot{y}_i + \dot{u}_l^2 x_i + \ddot{u}_l y_i + n_0^2 R_l - n_{if}^2(R_l + x_i)\ \ -2\dot{u}_l\dot{x}_i + \dot{u}_l^2 y_i - \ddot{u}_l x_i - n_{if}^2 y_i\ \ -n_{if}^2 z_i]^{\mathrm{T}}$ and $\tilde{\boldsymbol{U}}_i = [u_{ix}\ 0\ u_{iz}]^{\mathrm{T}}$. u_l is the argument of latitude of the leader, R_l and $R_{if} = \sqrt{(R_l + x_i)^2 + y_i^2 + z_i^2}$ are the orbital radius of the leader and the follower, respectively. $n_0 = \sqrt{\mu_e / R_l^3}$ and $n_{if} = \sqrt{\mu_e / R_{if}^3}$, while μ_e is the gravitational constant of Earth. By defining $\boldsymbol{X}_i = [x_i\ y_i\ z_i\ \dot{y}_i\ \dot{x}_i\ \dot{z}_i]^{\mathrm{T}}$ as the relative state vector, equation (1) is generally linearized as [23]

$$\dot{\boldsymbol{X}}_i = \boldsymbol{A}\boldsymbol{X}_i + \boldsymbol{B}\boldsymbol{U}_i, \tag{2}$$

with

$$\boldsymbol{A} = \begin{bmatrix} 0 & 0 & 0 & 0 & 1 & 0 \\ 0 & 0 & 0 & 1 & 0 & 0 \\ 0 & 0 & 0 & 0 & 0 & 1 \\ 0 & 0 & 0 & 0 & -2n_0 & 0 \\ 3n_0^2 & 0 & 0 & 2n_0 & 0 & 0 \\ 0 & 0 & -n_0^2 & 0 & 0 & 0 \end{bmatrix},$$

$$\boldsymbol{B} = [\boldsymbol{0}_{2\times 4}\ \boldsymbol{I}_{2\times 2}]^{\mathrm{T}},$$

where $\boldsymbol{U}_i = [u_{ix}\ u_{iz}]^{\mathrm{T}}$. Using the rank criterion in linear system theory, the rank of controllability matrix for the system (2) is $5 < 6$ [11]. Therefore, we can conclude that the system is uncontrollable in the case without along-track thrust. Moreover, according to the linear system theory, the system could be recast into a controllable subspace $\bar{\boldsymbol{X}}_{ic} = [\dot{y}_i\ z_i\ y_i\ \dot{x}_i\ \dot{z}_i]^{\mathrm{T}}$ and an uncontrollable one $\bar{X}_{iu} = \frac{\dot{y}_i}{2n_0} + x_i$, governed by

$$\dot{\bar{\boldsymbol{X}}}_{ic} = \bar{\boldsymbol{A}}_{cc}\bar{\boldsymbol{X}}_{ic} + \bar{\boldsymbol{A}}_{cu}\bar{X}_{iu} + \bar{\boldsymbol{B}}_c\boldsymbol{U}_i, \tag{3}$$

with

$$\bar{\boldsymbol{A}}_{cc} = \begin{bmatrix} 0 & 0 & 0 & -2n_0 & 0 \\ 0 & 0 & 0 & 0 & 1 \\ 1 & 0 & 0 & 0 & 0 \\ n_0/2 & 0 & 0 & 0 & 0 \\ 0 & -n_0^2 & 0 & 0 & 0 \end{bmatrix},\ \bar{\boldsymbol{A}}_{cu} = \begin{bmatrix} 0 \\ 0 \\ 0 \\ 3n_0^2 \\ 0 \end{bmatrix},$$

$$\bar{\boldsymbol{B}}_c = [\ \boldsymbol{0}_{2\times 3}\quad \boldsymbol{I}_{2\times 2}\ ]^{\mathrm{T}}.$$

Despite that the system is uncontrollable, it does not hinder the feasibility of formation hovering. As analyzed in [11, 13], the uncontrollable state $\bar{X}_{iu}$ keeps its initial value during the whole hovering process from the initial time t_{i0} to the final time t_{if} and equals to the stability condition $2n_0x_i(t) + \dot{y}_i(t) = 0$ of the desired hovering configuration, that is,

$$\bar{X}_{iu}(t_{i0}) = \bar{X}_{iu}(t_{if}) = 0. \tag{4}$$

B. Feasible Initial Position

By definition of formation hovering, the follower is required to maintain a fixed position in the LVLH frame relative to the leader, namely, the first-order time derivative of the desired state $\boldsymbol{X}_{id}$ satisfies $\dot{\boldsymbol{X}}_{id} = [\dot{x}_{id}\ \dot{y}_{id}\ \dot{z}_{id}\ \ddot{x}_{id}\ \ddot{y}_{id}\ \ddot{z}_{id}]^{\mathrm{T}} = [\boldsymbol{0}_{1\times 6}]^{\mathrm{T}}$. With the loss of along-track input, the thrusts from the other two channels cannot ensure that the follower hovers at an arbitrary relative position. Hence, the initial state of the follower is also subject to the underactuated dynamics, as derived by the following theorem.

Theorem 1: For the case without along-track thrust, given that the initial relative velocity $\boldsymbol{v}_i(t_{i0}) = \boldsymbol{v}_{ig} = [\dot{x}_{ig}\ \dot{y}_{ig}\ \dot{z}_{ig}]^{\mathrm{T}}$ and the initial relative acceleration $\ddot{\boldsymbol{\rho}}_i(t_{i0}) = \ddot{\boldsymbol{\rho}}_{ig} = [0\ 0\ 0]^{\mathrm{T}}$, the feasible set of initial positions $\boldsymbol{\rho}_{ig}$ is expressed as

$$\boldsymbol{\Lambda}_{i1} = (\boldsymbol{\Lambda}_{i11} \cup \boldsymbol{\Lambda}_{i12}) \cap \boldsymbol{\Lambda}_{i13}, \tag{5}$$

where the detailed expressions of $\boldsymbol{\Lambda}_{i11}$, $\boldsymbol{\Lambda}_{i12}$, and $\boldsymbol{\Lambda}_{i13}$ are derived in the following.

Proof: Since the leader flies in a circular orbit, $\dot{u}_l = n_0$ and $\ddot{u}_l = 0$. As $\boldsymbol{u}_i = [u_{ix}\ 0\ u_{iz}]^{\mathrm{T}}$, substituting the initial state $\boldsymbol{X}_{ig} = [\boldsymbol{\rho}_{ig}^{\mathrm{T}}\ \boldsymbol{v}_{ig}^{\mathrm{T}}]^{\mathrm{T}} = [x_{ig}\ y_{ig}\ z_{ig}\ \dot{x}_{ig}\ \dot{y}_{ig}\ \dot{z}_{ig}]^{\mathrm{T}}$ and the desired state $\boldsymbol{X}_{id} = [\boldsymbol{\rho}_{id}^{\mathrm{T}}\ \boldsymbol{v}_{id}^{\mathrm{T}}]^{\mathrm{T}} = [x_{id}\ y_{id}\ z_{id}\ \dot{x}_{id}\ \dot{y}_{id}\ \dot{z}_{id}]^{\mathrm{T}}$ into the nonlinear dynamics (1) yields

$$\begin{cases} -2n_0\dot{y}_{ig} + (n_{if}^2 - n_0^2)(x_{ig} - x_{id}) = u_{ix}(t_{i0}), \\ 2n_0\dot{x}_{ig} + (n_{if}^2 - n_0^2)(y_{ig} - y_{id}) = 0, \\ n_{if}^2(z_{ig} - z_{id}) = u_{iz}(t_{i0}). \end{cases} \tag{6}$$

Provided that $\dot{x}_{ig} = 0$, the second term of (6) leads to $(n_{if}^2 - n_0^2)(y_{ig} - y_{id}) = 0$. If $n_{if}^2 - n_0^2 = 0$ holds, due to $n_0 = \sqrt{\mu_e/R_l^3}$ and $n_{if} = \sqrt{\mu_e/R_{if}^3}$, one has

$$R_{if}^2 = R_l^2. \tag{7}$$

In view of $R_{if}^2 = (R_l + x_{ig})^2 + y_{ig}^2 + z_{ig}^2 = x_{ig}^2 + y_{ig}^2 + z_{ig}^2 + 2R_l x_{ig} + R_l^2 = R_l^2$, a nonlinear feasible set of initial positions is thus formulated as

$$\boldsymbol{\Lambda}_{i11} = \{\boldsymbol{\rho}_{ig} | 2R_l x_{ig} + \|\boldsymbol{\rho}_{ig}\|^2 = 0\}. \tag{8}$$

If $y_{ig} - y_{id} = 0$ holds, another set could be solved as

$$\boldsymbol{\Lambda}_{i12} = \{\boldsymbol{\rho}_{ig} | y_{ig} = y_{id}\}. \tag{9}$$

Moreover, there also exists a linear constraint generated by (4), that is, $\dot{y}_{ig}/(2n_0) + x_{ig} = \dot{y}_{id}/(2n_0) + x_{id} = 0$. Given that $\dot{y}_{ig} \neq 0$ and $\dot{y}_{id} = 0$, a linear feasible set is expressed as

$$\boldsymbol{\Lambda}_{i13} = \{\boldsymbol{\rho}_{ig} | x_{ig} = x_{id} - \dot{y}_{ig}/(2n_0)\}. \tag{10}$$

Typically, the linearization error is less than 0.03% while $\|\boldsymbol{\rho}_i\| \leq 100$ km [12]. Since the position of the follower relative to the leader is negligible compared with the radius of their orbits, the nonlinear and linear sets (i.e., equations (8)-(10)) could be integrated into one set (5). Here completes the proof of Theorem 1. □

Remark 1: Since the orbital angular velocity of the leader remains constant during hovering, solving the equation $(n_{if}^2 - n_0^2)(y_{ig} - y_{id}) = 0$ can also yield $R_{if}^2 = (R_l + x_{id})^2 + y_{id}^2 + z_{id}^2$ and $y_{ig} - y_{id} = 0$. Likewise, two feasible sets of desired positions are, respectively, given by $\boldsymbol{\Lambda}_{i21} = \{\boldsymbol{\rho}_{id} | 2R_l x_{id} + \|\boldsymbol{\rho}_{id}\|^2 = 0\}$ and $\boldsymbol{\Lambda}_{i22} = \{\boldsymbol{\rho}_{id} | y_{id} = y_{ig}\}$. In the light of (4), the linear feasible set has the expression of $\boldsymbol{\Lambda}_{i23} = \{\boldsymbol{\rho}_{id} | x_{id} = x_{ig} + \dot{y}_{ig}/(2n_0)\}$. Thus, the feasible set of desired positions can be summarized as $(\boldsymbol{\Lambda}_{i21} \cup \boldsymbol{\Lambda}_{i22}) \cap \boldsymbol{\Lambda}_{i23}$.

Remark 2: According to (6), if $\dot{x}_{ig} = 0$ holds, the feasible set of initial positions satisfies the same nonlinear condition as that of the desired ones. In other words, the follower hovers from one position to another one. If $\dot{x}_{ig} \neq 0$, it can be seen that the feasible set of desired positions can be derived through the initial velocity and position, but the initial state can not be obtained via the desired position. For the linear set (10), if $\dot{y}_{ig} \neq 0$, given one of the initial radial position or desired radial one, the other could be solved by the linear condition (4), corresponding that the follower flies from a natural orbit around the leader to a specified hovering position.

Remark 3: For the case without radial control, since $\boldsymbol{u}_i = [0\ u_{iy}\ u_{iz}]^{\mathrm{T}}$, the equation $-2n_0\dot{y}_{ig} + (n_{if}^2 - n_0^2)(x_{ig} - x_{id}) = 0$ can be deduced from the first term of (6). Provided that $\dot{y}_{ig} = 0$, by using similar approaches in Theorem 1, the feasible sets of initial and desired positions for the case without radial thrust could be, respectively, derived as $\boldsymbol{\Lambda}_{i3} = \{\boldsymbol{\rho}_{ig} | 2R_l x_{ig} + \|\boldsymbol{\rho}_{ig}\|^2 = 0\} \cup \{\boldsymbol{\rho}_{ig} | x_{ig} = x_{id}\}$ and $\boldsymbol{\Lambda}_{i4} = \{\boldsymbol{\rho}_{id} | 2R_l x_{id} + \|\boldsymbol{\rho}_{id}\|^2 = 0\} \cup \{\boldsymbol{\rho}_{id} | x_{id} = x_{ig}\}$. As can be seen, the forms of the nonlinear feasible sets for both underactuated cases are the same, indicating these sets are subject to the same dynamics constraint. In addition, the reason why there is no linear set similar to (10) in $\boldsymbol{\Lambda}_{i3}$ and $\boldsymbol{\Lambda}_{i4}$ is that the system is controllable in this underactuated case. Hence, the feasible set without radial thrust can be regarded as a subset of that for the case without along-track thrust.

C. Problem Statement

The control objective of the underactuated spacecraft formation hovering problem considered in this brief is to present a synchronization control scheme, which designs the initial and desired positions for hovering from the aforementioned feasible sets, such that the controller could eliminate the initial offsets in the presence of unmatched disturbances and synchronize the motion between followers simultaneously.

III. Synchronization Controller Design

Actually, the spacecraft may drift from the hovering position due to the J_2 perturbation, atmospheric drag, and linearization errors. Thus, the perturbed nonlinear dynamical system of formation hovering can be formulated as

$$\dot{\boldsymbol{X}}_i = \boldsymbol{A}\boldsymbol{X}_i + \boldsymbol{B}\boldsymbol{U}_i + \Delta\tilde{\boldsymbol{F}}_i(\boldsymbol{X}_i) + \tilde{\boldsymbol{d}}_i, \tag{11}$$

where $\Delta\tilde{\boldsymbol{F}}(\boldsymbol{X}_i) = \tilde{\boldsymbol{F}}(\boldsymbol{X}_i) - \boldsymbol{A}\boldsymbol{X}_i$ is defined as the linearization error, $\tilde{\boldsymbol{F}}_i(\boldsymbol{X}_i) = [\boldsymbol{0}_{1\times 3}\ f_y\ f_x\ f_z]^{\mathrm{T}}$, and $\tilde{\boldsymbol{d}}_i = [\boldsymbol{0}_{1\times 3}\ \tilde{d}_y\ \tilde{d}_x\ \tilde{d}_z]^{\mathrm{T}}$ is denoted as the external disturbance. Since $\dot{\boldsymbol{X}}_{id} = \boldsymbol{0}_{6\times 1}$ and $\boldsymbol{B}^{\mathrm{T}}\boldsymbol{B} = \boldsymbol{I}_{2\times 2}$ hold [13], the continuous open-loop control at $\boldsymbol{\rho}_{id}$ can be solved by (11) , one has

$$\boldsymbol{u}_{id} = \boldsymbol{B}^{\mathrm{T}}(\boldsymbol{A}\boldsymbol{X}_{id} + \Delta\tilde{\boldsymbol{F}}_i(\boldsymbol{X}_{id})). \tag{12}$$

We express $\boldsymbol{e}_i = \boldsymbol{X}_i - \boldsymbol{X}_{id}$ as the error state and $\boldsymbol{u}_i = \boldsymbol{U}_i - \boldsymbol{u}_{id}$ as the error control input, the error dynamics of

formation hovering is then governed by

$$\dot{\boldsymbol{e}}_i = \boldsymbol{A}\boldsymbol{e}_i + \boldsymbol{B}\boldsymbol{u}_i + \boldsymbol{d}_i, \tag{13}$$

where $\boldsymbol{d}_i = \Delta\tilde{\boldsymbol{F}}_i(\boldsymbol{X}_i) - \Delta\tilde{\boldsymbol{F}}_i(\boldsymbol{X}_{id}) + \tilde{\boldsymbol{d}}_i = [0_{1\times3}\ d_y\ d_x\ d_z]^{\mathrm{T}}$, satisfying $\|\boldsymbol{d}_i\| \le d_{im}$ and $d_{im} > 0$.

A. Controller Design

Different from the works in [11–14], the underactuated error dynamics have the new decomposition expression of

$$\begin{cases} \dot{\tilde{\boldsymbol{e}}}_{i\rho} = \boldsymbol{A}_{11}\tilde{\boldsymbol{e}}_{i\rho} + \boldsymbol{A}_{12}\boldsymbol{e}_{iv} + \boldsymbol{d}_{i\rho}, \\ \dot{\boldsymbol{e}}_{iv} = \boldsymbol{A}_{13}e_{i\rho} + \boldsymbol{A}_{14}e_{iv} + \boldsymbol{u}_i + \boldsymbol{d}_{iv}, \end{cases} \tag{14}$$

with

$$\begin{aligned} \boldsymbol{A}_{11} &= \begin{bmatrix} 0 & 1 & 0 \\ 0 & 0 & 0 \\ 0 & 0 & 0 \end{bmatrix},\ \boldsymbol{A}_{12} = \begin{bmatrix} 0 & 0 \\ -2n_0 & 0 \\ 0 & 1 \end{bmatrix}, \\ \boldsymbol{A}_{13} &= \begin{bmatrix} 2n_0 & 3n_0^2 & 0 \\ 0 & 0 & -n_0^2 \end{bmatrix},\ \boldsymbol{A}_{14} = [\boldsymbol{0}_{2\times2}], \end{aligned} \tag{15}$$

where $\boldsymbol{e}_{i\rho} = [\dot{e}_{iy}\ e_{ix}\ e_{iz}]^{\mathrm{T}}$, $\tilde{\boldsymbol{e}}_{i\rho} = [e_{iy}\ \dot{e}_{iy}\ e_{iz}]^{\mathrm{T}}$, $\boldsymbol{e}_{iv} = [\dot{e}_{ix}\ \dot{e}_{iz}]^{\mathrm{T}}$, $\boldsymbol{u}_i = [u_{ix}\ u_{iz}]^{\mathrm{T}}$, $\boldsymbol{d}_{i\rho} = [0\ d_{iy}\ 0]^{\mathrm{T}}$, and $\boldsymbol{d}_{iv} = [d_{ix}\ d_{iz}]^{\mathrm{T}}$. Note that the vector $\boldsymbol{u}_i \in \mathbb{R}^2$ and $\boldsymbol{e}_{iv} \in \mathbb{R}^2$, but $\tilde{\boldsymbol{e}}_{i\rho} \in \mathbb{R}^3$. To make the degree of freedom of $\tilde{\boldsymbol{e}}_{i\rho}$ consistent with that of $\boldsymbol{u}_i$, a linear transformation is conducted on $\tilde{\boldsymbol{e}}_{i\rho}$.

$$\bar{\boldsymbol{e}}_{i\rho} = \boldsymbol{P}_{11}\tilde{\boldsymbol{e}}_{i\rho}, \tag{16}$$

with

$$\boldsymbol{P}_{11} = \begin{bmatrix} a_1 & b_1 & 0 \\ 0 & 0 & f_1 \end{bmatrix}, \tag{17}$$

where a_1, b_1, and f_1 are constants to be set.

Then, taking the time derivative of $\bar{\boldsymbol{e}}_{i\rho}$ yields $\dot{\bar{\boldsymbol{e}}}_{i\rho} = \boldsymbol{P}_{11}\dot{\tilde{\boldsymbol{e}}}_{i\rho} = \boldsymbol{P}_{11}(\boldsymbol{A}_{11}\tilde{\boldsymbol{e}}_{i\rho} + \boldsymbol{A}_{12}\boldsymbol{e}_{iv} + \boldsymbol{d}_{i\rho})$. It can be seen that by using $\boldsymbol{P}_{11}$, the along-track error vector is in the same channel as the radial one. As a result, the disturbance in the along-track direction enters the system through the radial channel, producing the unmatched disturbances. To eliminate the influence of the unmatched disturbances on the control accuracy, a disturbance observer proposed in [24] is introduced to estimate the real value of the unmatched disturbance for designing the underactuated controller.

Assumption 1: The external disturbance $\boldsymbol{d}_i$ and its derivatives are bounded, satisfying $\|\boldsymbol{d}_i\| \le d_{im}$ and $\|\dot{\boldsymbol{d}}_i(t)\| \le d_{if}$, respectively [24].

Lemma 1: [24] Define $\boldsymbol{z}_{i1}$, $\boldsymbol{z}_{i2}$, and $\boldsymbol{z}_{i3} = \hat{\boldsymbol{d}}_i$ as the estimated values of $\boldsymbol{x}_{i1} = \boldsymbol{\rho}_i$, $\boldsymbol{x}_{i2} = \boldsymbol{v}_i$, and $\boldsymbol{x}_{i3} = \boldsymbol{d}_i$, respectively, the finite-time convergent extended state observer is constructed as

$$\begin{cases} \dot{\boldsymbol{z}}_{i1} = \boldsymbol{z}_{i2} - \kappa_{11}\mathrm{sig}^{(\kappa_{14}+1)/2}(\boldsymbol{\varepsilon}_{i1}), \\ \dot{\boldsymbol{z}}_{i2} = \boldsymbol{z}_{i3} - \kappa_{12}\mathrm{sig}^{(\kappa_{14}+1)/2}(\boldsymbol{\varepsilon}_{i1}) + \tilde{\boldsymbol{U}}_i, \\ \dot{\boldsymbol{z}}_{i3} = -\kappa_{13}\mathrm{sig}^{\kappa_{14}}(\boldsymbol{\varepsilon}_{i1}), \end{cases} \tag{18}$$

where $\dot{\boldsymbol{\varepsilon}}_{i1} = \boldsymbol{\varepsilon}_{i2} - \kappa_{11}\mathrm{sig}^{(\kappa_{14}+1)/2}(\boldsymbol{\varepsilon}_{i1})$, $\dot{\boldsymbol{\varepsilon}}_{i2} = \boldsymbol{\varepsilon}_{i3} - \kappa_{12}\mathrm{sig}^{(\kappa_{14}+1)/2}(\boldsymbol{\varepsilon}_{i1})$, and $\dot{\boldsymbol{\varepsilon}}_{i3} = -\kappa_{13}\mathrm{sig}^{(\kappa_{14}+1)/2}(\boldsymbol{\varepsilon}_{i1}) - \dot{\boldsymbol{x}}_{i3}$. The terms $\boldsymbol{\varepsilon}_{i1} = \boldsymbol{z}_{i1} - \boldsymbol{x}_{i1}$, $\boldsymbol{\varepsilon}_{i2} = \boldsymbol{z}_{i2} - \boldsymbol{x}_{i2}$, and $\boldsymbol{\varepsilon}_{i3} = \boldsymbol{z}_{i3} - \boldsymbol{x}_{i3}$ with the bound as $\|\boldsymbol{\varepsilon}_{i3}\| \le \varepsilon_{im} = \|\hat{\boldsymbol{d}}_i - \boldsymbol{d}_i\|$. $\kappa_{11} > 0$, $\kappa_{12} > 0$, $\kappa_{13} > 0$, and $0 < \kappa_{14} < 1$ are observer gains.

It is assumed that every follower can accurately obtain its position and velocity information. Thus, only the external disturbance $\boldsymbol{d}_i$ and its time derivative $\dot{\boldsymbol{d}}_i$ need to be estimated. A non-singular fast terminal sliding mode (NFTSM) function is designed as

$$\boldsymbol{s}_i = \alpha_1\bar{\boldsymbol{e}}_{i\rho} + \chi_1\dot{\bar{\boldsymbol{e}}}_{i\rho} + \beta_1\dot{\bar{\boldsymbol{e}}}_{i\rho}^{\,q_1/p_1}, \tag{19}$$

where $\alpha_1 > 0$, $\chi_1 > 0$, and $\beta_1 > 0$ are constants. q_1 and p_1 are odd integers, satisfying $p_1 < q_1 < 2p_1$.

Let $\dot{\boldsymbol{s}}_i = 0$, the equivalent control $\boldsymbol{u}_{i1}$ is thus obtained as

$$\begin{aligned} \boldsymbol{u}_{i1} = &-\boldsymbol{S}^{-1}\boldsymbol{H}_i - \boldsymbol{S}^{-1}[\chi_1\boldsymbol{P}_{11}(\chi_1^{-1}\alpha_1(\boldsymbol{A}_{11}\tilde{\boldsymbol{e}}_{i\rho} + \boldsymbol{A}_{12}\boldsymbol{e}_{iv}) \\ &+ \boldsymbol{A}_{11}(\boldsymbol{A}_{11}\tilde{\boldsymbol{e}}_{i\rho} + \boldsymbol{A}_{12}\boldsymbol{e}_{iv}) + \boldsymbol{A}_{12}\boldsymbol{A}_{13}\boldsymbol{e}_{i\rho}) \\ &+ \tilde{\boldsymbol{P}}_{11}\boldsymbol{P}_{11}(\boldsymbol{A}_{11}(\boldsymbol{A}_{11}\tilde{\boldsymbol{e}}_{i\rho} + \boldsymbol{A}_{12}\boldsymbol{e}_{iv}) + \boldsymbol{A}_{12}\boldsymbol{A}_{13}\boldsymbol{e}_{i\rho})], \end{aligned} \tag{20}$$

where $\bar{\boldsymbol{P}}_{11} = \beta_1 q_1/p_1(\boldsymbol{P}_{11}(\boldsymbol{A}_{11}\tilde{\boldsymbol{e}}_{i\rho} + \boldsymbol{A}_{12}\boldsymbol{e}_{iv}))^{(q_1/p_1)-1} = [p_{11}\ p_{12}]^{\mathrm{T}}$, $\tilde{\boldsymbol{P}}_{11} = \mathrm{diag}(p_{11},\ p_{12})$, $\boldsymbol{S} = \chi_1\boldsymbol{P}_{11}\boldsymbol{A}_{12} + \tilde{\boldsymbol{P}}_{11}\boldsymbol{P}_{11}\boldsymbol{A}_{12}$, and $\boldsymbol{H}_i = \chi_1\boldsymbol{P}_{11}(\alpha_1\chi_1^{-1}\hat{\boldsymbol{d}}_{i\rho} + \boldsymbol{A}_{11}\hat{\boldsymbol{d}}_{i\rho} + \dot{\hat{\boldsymbol{d}}}_{i\rho} + \boldsymbol{A}_{12}\hat{\boldsymbol{d}}_{iv}) + \tilde{\boldsymbol{P}}_{11}\boldsymbol{P}_{11}(\boldsymbol{A}_{11}\hat{\boldsymbol{d}}_{i\rho} + \boldsymbol{A}_{12}\hat{\boldsymbol{d}}_{iv} + \dot{\hat{\boldsymbol{d}}}_{i\rho})$ is the estimated value of the unmatched disturbance $\boldsymbol{\delta}_i = \chi_1\boldsymbol{P}_{11}(\alpha_1\chi_1^{-1}\boldsymbol{d}_{i\rho} + \boldsymbol{A}_{11}\boldsymbol{d}_{i\rho} + \dot{\boldsymbol{d}}_{i\rho} + \boldsymbol{A}_{12}\boldsymbol{d}_{iv}) + \tilde{\boldsymbol{P}}_{11}\boldsymbol{P}_{11}(\boldsymbol{A}_{11}\boldsymbol{d}_{i\rho} + \boldsymbol{A}_{12}\boldsymbol{d}_{iv} + \dot{\boldsymbol{d}}_{i\rho})$, namely, the terms $\hat{\boldsymbol{d}}_{i\rho}$, $\dot{\hat{\boldsymbol{d}}}_{i\rho}$, and $\hat{\boldsymbol{d}}_{iv}$ are the estimated values of $\boldsymbol{d}_{i\rho}$, $\dot{\boldsymbol{d}}_{i\rho}$, and $\boldsymbol{d}_{iv}$, respectively. Thus, two conclusions on $\boldsymbol{\delta}_i$ can thus be obtained: 1) $\boldsymbol{\delta}_i$ is composed of the algebraic sum of several matched disturbances. 2) The bounded value of $\boldsymbol{\delta}_i$ is larger than that of the matched disturbance, thus highlighting the necessity of introducing a disturbance observer.

Subsequently, a switch control is selected as $\boldsymbol{u}_{i2} = -k_1\boldsymbol{s}_i - k_2\mathrm{sig}^{\gamma_1}(\boldsymbol{s}_i)$, where $k_1 > 0$, $k_2 > 0$, and $0 < \gamma_1 < 1$ are constants. The disturbances observer-based NFTSM controller (DO-NFTSMC) for the case without along-track thrust is then expressed as

$$\boldsymbol{u}_i' = \boldsymbol{u}_{i1} + \boldsymbol{u}_{i2} + \boldsymbol{u}_{id}. \tag{21}$$

Different from DO-NFTSMC, NFTSM controller (NFTSM-C) only uses the bound of $\boldsymbol{\delta}_i$, and the design process is not presented here. Notably, DO-NFTSMC (21) only concerns the hovering control for a single follower but does not consider the synchronization motion control between the followers. By defining the synchronization error as $\boldsymbol{s}_i - \boldsymbol{s}_j$, where $\boldsymbol{s}_i$ and $\boldsymbol{s}_j$ are the sliding surface of the ith and jth $(i, j = 1, 2, ..., n,\ i \ne j)$ followers, respectively. A sliding-mode-based synchronization hovering item is given by

$$\boldsymbol{u}_{i3} = -k_3\sum_{j=1}^{n} w_{ij}(\boldsymbol{s}_i - \boldsymbol{s}_j), \tag{22}$$

where $k_3 > 0$ is a constant and w_{ij} is an element within the matrix $\mathcal{W}$. Throughout this paper, the undirected graph $\mathcal{G}$ is a topology composed of n followers, where $\mathcal{W}$ and $\mathcal{L}$ are the adjacency matrix and the Laplace matrix of $\mathcal{G}$, respectively [25]. It is to be noted that $\mathcal{L}$ is a positive semidefinite matrix.

Therefore, the synchronization controller (SC) can be summarized as

$$\boldsymbol{u}_i = \boldsymbol{u}_{i1} + \boldsymbol{u}_{i2} + \boldsymbol{u}_{i3} + \boldsymbol{u}_{id}. \tag{23}$$

For the convenience of the readers to understand the operation mechanism of the underactuated synchronization control scheme proposed in this paper, the schematic diagram of the whole scheme is depicted in Fig. 1.

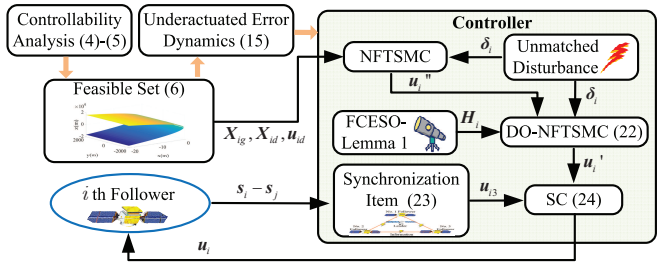

Fig. 1. Schematic diagram of synchronization control scheme.

B. Convergence Analysis

Before analyzing the convergence of the closed-loop system, two lemmas are given.

Lemma 2: [26] Assume V_1 is a positive function, one has

$$\dot{V}_1 + \alpha_1 V_1 + \alpha_2 {V_1}^{\alpha_3} \leqslant 0, \tag{24}$$

where $\alpha_1 > 0$, $\alpha_2 > 0$, and $0 < \alpha_3 < 1$ are constants, V_1 will converge to zero in a finite time $t_1 \leqslant \frac{1}{\alpha_1(1-\alpha_3)} \ln \frac{\alpha_1 {V_1}^{1-\alpha_3}(t_{i0})+\alpha_2}{\alpha_2}$.

Lemma 3: [12] Let $\dot{\boldsymbol{x}} = \boldsymbol{f}(t, \boldsymbol{x})$ be a nominal system with exponentially stable equilibrium point $\boldsymbol{x} = 0$. Let $V_2(t, \boldsymbol{x})$ be a Lyapunov function of the system and satisfies these conditions.

$$\begin{cases} \sigma_1 \|\boldsymbol{x}\|^2 \leqslant V_2(t, \boldsymbol{x}) \leqslant \sigma_2 \|\boldsymbol{x}\|^2, \\ \frac{\partial V_2}{\partial \boldsymbol{x}} + \frac{\partial V_2}{\partial t} \boldsymbol{f}(t, \boldsymbol{x}) \leqslant -\sigma_3 \|\boldsymbol{x}\|^2, \\ \| \frac{\partial V_2}{\partial \boldsymbol{x}} \| \leqslant \sigma_4 \|\boldsymbol{x}\|, \end{cases} \tag{25}$$

where $(t, \boldsymbol{x}) \in [0, \infty) \times D$ and $\sigma_\lambda (\lambda = 1, ..., 4) > 0$. $\boldsymbol{g}(t, \boldsymbol{x})$ is defined as the vanishing perturbation and satisfies

$$\begin{cases} \|\boldsymbol{g}(t, \boldsymbol{x})\| \leqslant \varrho \|\boldsymbol{x}\|, \\ \varrho < \sigma_3 / \sigma_4. \end{cases} \tag{26}$$

Hence, $\boldsymbol{x} = 0$ is an exponentially stable equilibrium point of the perturbed nominal system $\dot{\boldsymbol{x}} = \boldsymbol{f}(t, \boldsymbol{x}) + \boldsymbol{g}(t, \boldsymbol{x})$.

Lemma 3 only applies to the exponentially stable case. For the sliding surface $\boldsymbol{s}_i$ in (19), it generally converges to the equilibrium point in finite time. Consequently, we extend this lemma to the finite-time case, given by the following corollary.

Corollary 1: Let $\dot{\boldsymbol{x}} = \boldsymbol{f}(t, \boldsymbol{x})$ be a nominal system with finite-time stable equilibrium point $\boldsymbol{x} = 0$. Let $V_2(t, \boldsymbol{x})$ be a Lyapunov function of the system and satisfies these conditions.

$$\begin{cases} \sigma_1 \|\boldsymbol{x}\|^2 \leqslant V_2(t, \boldsymbol{x}) \leqslant \sigma_2 \|\boldsymbol{x}\|^2, \\ \frac{\partial V_2}{\partial \boldsymbol{x}} + \frac{\partial V_2}{\partial t} \boldsymbol{f}(t, \boldsymbol{x}) \leqslant -\sigma_3 \|\boldsymbol{x}\|^2 - \sigma_4 \|\boldsymbol{x}\|^{\gamma_2 + 1}, \\ \| \frac{\partial V_2}{\partial \boldsymbol{x}} \| \leqslant \sigma_5 \|\boldsymbol{x}\|, \end{cases} \tag{27}$$

where $(t, \boldsymbol{x}) \in [0, \infty) \times D$, $\sigma_\lambda (\lambda = 1, ..., 5) > 0$, and $0 < \gamma_2 < 1$. $\boldsymbol{g}(t, \boldsymbol{x})$ is denoted as a vanishing perturbation that satisfies

$$\begin{cases} \|\boldsymbol{g}(t, \boldsymbol{x})\| \leqslant \varrho \|\boldsymbol{x}\|, \\ \varrho < \sigma_3 / \sigma_5. \end{cases} \tag{28}$$

Then, $\boldsymbol{x} = 0$ is a finite-time stable equilibrium point of the perturbed nominal system $\dot{\boldsymbol{x}} = \boldsymbol{f}(t, \boldsymbol{x}) + \boldsymbol{g}(t, \boldsymbol{x})$.

Proof: Substituting the first term of (27) into the second term leads to

$$\dot{V}_2 = \frac{\partial V_2}{\partial \boldsymbol{x}} + \frac{\partial V_2}{\partial t} \boldsymbol{f}(t, \boldsymbol{x}) \leq -\frac{\sigma_3}{\sigma_2} V_2 - \frac{\sigma_4}{{\sigma_2}^{\frac{\gamma_2+1}{2}}} {V_2}^{\frac{\gamma_2+1}{2}}. \tag{29}$$

According to Lemma 2, $\boldsymbol{x} = 0$ is thus regarded as the finite-time stable equilibrium point of $\dot{\boldsymbol{x}} = \boldsymbol{f}(t, \boldsymbol{x})$. For the perturbed system $\dot{\boldsymbol{x}} = \boldsymbol{f}(t, \boldsymbol{x}) + \boldsymbol{g}(t, \boldsymbol{x})$, the derivative of V_2 can be formulated as

$$\dot{V}_2 \leqslant \frac{\partial V_2}{\partial t} + \frac{\partial V_2}{\partial \boldsymbol{x}} \boldsymbol{f}(t, \boldsymbol{x}) + \| \frac{\partial V_2}{\partial \boldsymbol{x}} \| \|\boldsymbol{g}(t, \boldsymbol{x})\|. \tag{30}$$

Furthermore, substituting (27) into (30) yields

$$\frac{\partial V_2}{\partial t} + \frac{\partial V_2}{\partial \boldsymbol{x}} \boldsymbol{f}(t, \boldsymbol{x}) \leqslant -(\sigma_3 - \varrho \sigma_5) \|\boldsymbol{x}\|^2 - \sigma_4 \|\boldsymbol{x}\|^{\gamma_2 + 1}. \tag{31}$$

From Lemma 2, the perturbed nominal system $\dot{\boldsymbol{x}} = \boldsymbol{f}(t, \boldsymbol{x}) + \boldsymbol{g}(t, \boldsymbol{x})$ is finite-time stable if $\varrho < \sigma_3 / \sigma_5$ holds. This completes the proof. □

Next, we will discuss the convergence of the closed-loop system, especially the influence of the synchronization hovering item (22) on the system states.

Theorem 2: For the underactuated error dynamics (14), given that the sliding surface and the controller are designed as (19) and (23), respectively. If $\sum_{j=1}^{n} |\phi'(l_{ij})| \leq \kappa_l \|\boldsymbol{s}_i\|$ and $b_1/a_1 > 0$ hold, the system will converge to the desired hovering position in finite time, and the stable hovering accuracy can be expressed as

$$\|\boldsymbol{s}_i\| \leq \Delta_{\boldsymbol{s}_i}, \ |e_{i\mu}| \leq \Delta_{e_{i\mu}}, \ \mu = x, y, z, \tag{32}$$

where $\kappa_l > 0$ is a constant. The detailed expressions of $\phi'(l_{ij})$, l_{ij}, $\Delta_{\boldsymbol{s}_i}$, and $\Delta_{e_{i\mu}}$ will be derived in the following.

Proof: Substituting (23) into the time derivative of $\boldsymbol{s}_i$ yields

$$\dot{\boldsymbol{s}}_i = \boldsymbol{f}_i + \boldsymbol{g}_i + \boldsymbol{\Delta}_i, \tag{33}$$

where $\boldsymbol{f}_i = \boldsymbol{u}_{i2}$, $\boldsymbol{g}_i = \boldsymbol{u}_{i3}$, and $\boldsymbol{\Delta}_i = \boldsymbol{H}_i - \boldsymbol{\delta}_i$ is the observation error with its bound $\|\boldsymbol{\Delta}_i\| = \|\boldsymbol{H}_i - \boldsymbol{\delta}_i\| \leq \Delta_{im}$.

From Corollary 1, it can be concluded that $\boldsymbol{e}_i = 0$, $\boldsymbol{s}_i = 0$, and $\boldsymbol{g}_i = 0$ at the desired hovering position $\boldsymbol{\rho}_{id}$. $\boldsymbol{g}_i$ is thus regarded as a vanishing disturbance of the nominal system $\dot{\boldsymbol{s}}_i = \boldsymbol{f}_i$. For the nominal system $\dot{\boldsymbol{s}}_i = \boldsymbol{f}_i$ perturbed by $\boldsymbol{\Delta}_i$, considering a Lyapunov candidate $V_{i1} = \frac{1}{2} \boldsymbol{s}_i^{\mathrm{T}} \boldsymbol{s}_i$ and taking its time derivative yields

$$\dot{V}_{i1} = \boldsymbol{s}_i^{\mathrm{T}} (\boldsymbol{f}_i + \boldsymbol{\Delta}_i) \leq -k_1 \|\boldsymbol{s}_i\|^2 - k_2 \|\boldsymbol{s}_i\|^{\gamma_1 + 1} + \|\boldsymbol{s}_i\| \Delta_{im}. \tag{34}$$

With regard to Corollary 1, setting the parameters as $\sigma_1 \in (0, 1/2], \sigma_2 \in [1/2, +\infty], \sigma_3 = k_1, \sigma_4 = k_2$, and $\sigma_5 = 1$, respectively. From (34), if the nominal system $\dot{\boldsymbol{s}}_i = \boldsymbol{f}_i$ holds $\boldsymbol{d}_i = 0$, that is, $\Delta_{im} = 0$. Then, $\boldsymbol{s}_i = 0$ is the finite-time stable equilibrium point by using the lemma 2. However, the system is actually perturbed by $\boldsymbol{\delta}_i$, and the corresponding observation error $\boldsymbol{\Delta}_i \neq 0$. By using the similar approaches in [26], it could be concluded that the second term of (27) is kept if $k_2 - \Delta_{im} \|\boldsymbol{s}_i\|^{-\gamma_1} > 0$ or $k_1 - \Delta_{im} \|\boldsymbol{s}_i\|^{-1} > 0$ holds. Thus, the other two terms within (27) could also be satisfied when the parameters $\sigma_\lambda (\lambda = 1, ..., 5)$ are selected above.

By denoting $\phi(l_{ij})$ as a smooth and nonnegative potential-like function [27], where $l_{ij} = \|\boldsymbol{s}_i - \boldsymbol{s}_j\|$ and $\phi'(l_{ij}) = \mathrm{d}\phi(l_{ij}) / \mathrm{d}l_{ij} = k_3 w_{ij} l_{ij}$. Thus, equation (22) has the expression of

$$\boldsymbol{g}_i = \boldsymbol{u}_{i3} = -\sum_{j=1}^{n} \phi'(l_{ij}) l_{ij}^{-1} (\boldsymbol{s}_i - \boldsymbol{s}_j). \tag{35}$$

Given that $\|l_{ij}^{-1}(\boldsymbol{s}_i-\boldsymbol{s}_j)\|=1$ and the term $\sum_{j=1}^{n}|\phi'(l_{ij})|\leq \kappa_l\|\boldsymbol{s}_i\|$ hold, equation (35) could be reduced to

$$\|\boldsymbol{g}_i\|\leq\sum_{j=1}^{n}|\phi'(l_{ij})|\leq\kappa_l\|\boldsymbol{s}_i\|. \tag{36}$$

Let $\varrho<\kappa_l\leq k_1=\sigma_3/\sigma_5$, both terms in (28) are satisfied. In this way, all the conditions in (27) and (28) are satisfied. Since the existence of the unmatched disturbance and the observer can not fully estimate the true value of the disturbance, $\boldsymbol{s}_i$ can only converge to a neighbourhood around the equilibrium, given by

$$\|\boldsymbol{s}_i\|\leq\Delta_{\boldsymbol{s}_i}=\min\left\{\left(k_2^{-1}\Delta_{im}\right)^{1/\gamma_1},\ k_1^{-1}\Delta_{im}\right\}. \tag{37}$$

For the case without disturbance observer, the system trajectory will converge to the region as $\Delta'_{\boldsymbol{s}_i}=\min\left\{\left(k_2^{-1}\delta_{im}\right)^{1/\gamma_1},\ k_1^{-1}\delta_{im}\right\}$, where δ_{im} is the bound of $\boldsymbol{\delta}_i$. Since $\Delta_{im}\ll\delta_{im}$, $\Delta_{\boldsymbol{s}_i}\ll\Delta_{\boldsymbol{s}'_i}$ holds. In addition, equation (37) shows that $\boldsymbol{g}_i$ will not disappear completely in the later stage of hovering because $\boldsymbol{s}_i$ cannot converge to the equilibrium. Notably, the bound of $\boldsymbol{g}_i$ composed of the algebraic sum of multiple sliding surfaces are of the same order of magnitude as the bound of $\Delta_{\boldsymbol{s}_i}$ and could be considered vanished, which satisfies the conditions within Corollary 1. Therefore, at the later stage of formation hovering, $\boldsymbol{f}_i$ is revised as $\boldsymbol{f}'_i=\boldsymbol{f}_i+\boldsymbol{g}_i$. Then, considering another Lyapunov candidate function $V_i=\sum_{i=1}^{n}V_{i1}=\frac{1}{2}\sum_{i=1}^{n}\boldsymbol{s}_i^{\mathrm{T}}\boldsymbol{s}_i$ and taking its time derivative yields

$$\begin{aligned}\dot{V}_i\leq&\sum_{i=1}^{n}\Delta_{im}\|\boldsymbol{s}_i\|-\sum_{i=1}^{n}k_1\|\boldsymbol{s}_i\|^2-\sum_{i=1}^{n}k_2\|\boldsymbol{s}_i\|^{\gamma_1+1}\\&-k_3\boldsymbol{F}^{\mathrm{T}}\mathcal{L}\boldsymbol{F}.\end{aligned} \tag{38}$$

where $\boldsymbol{F}=[\boldsymbol{s}_1^{\mathrm{T}},\ \boldsymbol{s}_2^{\mathrm{T}},\ \ldots,\boldsymbol{s}_n^{\mathrm{T}}]^{\mathrm{T}}$. By similar approaches, if $k_2-(2V_i)^{-(\gamma_1)/2}\Delta_{im}>0$ or $l_1-(2V_i)^{-1/2}\Delta_{im}>0$ holds, $\boldsymbol{s}_i$ converges to the region as

$$\|\boldsymbol{s}_i\|\leq\Delta_{\boldsymbol{s}_i}=\min\left\{\left(k_2^{-1}\Delta_{im}\right)^{1/\gamma_1},\ l_1^{-1}\Delta_{im}\right\}. \tag{39}$$

where $l_1=k_1+k_3\lambda_{\min}(\mathcal{L})$. As can be seen, equation (39) reveals that the minimum nonzero eigenvalue $\lambda_{\min}(\mathcal{L})$ of the Laplace matrix also affects the convergence accuracy of the system. Then, according to (19), the system dynamical equation is governed by $\alpha_1\bar{e}_{i\rho\eta}+\chi_1\dot{\bar{e}}_{i\rho\eta}+\beta_1\dot{\bar{e}}_{i\rho\eta}{}^{q_1/p_1}-\zeta_{i1\eta}=\zeta_{i2\eta}$, where $|\zeta_{i2\eta}|<\Delta_{\boldsymbol{s}_i}$, $\boldsymbol{\zeta}_{i1}=[\zeta_{i11}\ \zeta_{i12}]^{\mathrm{T}}=\chi_1\boldsymbol{P}_{11}\hat{\boldsymbol{d}}_{i\rho}+\beta_1(\dot{\tilde{\boldsymbol{e}}}_{i\rho})^{q_1/p_1}-\beta_1(\boldsymbol{P}_{11}(\boldsymbol{A}_{11}\tilde{\boldsymbol{e}}_{i\rho}+\boldsymbol{A}_{12}\boldsymbol{e}_{iv}))^{q_1/p_1}$ is bounded by $||\boldsymbol{\zeta}_{i1}||\leq\zeta_{iq}$, and the subscript $\eta=1,2$. Likewise, if $\chi_1-\frac{\zeta_{i1\eta}+\zeta_{i2\eta}}{\dot{\bar{e}}_{i\rho\eta}}>0$ or $\beta_1-\frac{\zeta_{i1\eta}+\zeta_{i2\eta}}{\dot{\bar{e}}_{i\rho\eta}{}^{q_1/p_2}}>0$ holds, $\dot{\bar{e}}_{i\rho\eta}$ and $\bar{e}_{i\rho\eta}$ converge, respectively, to the bounded regions as

$$\begin{cases}|\dot{\bar{e}}_{i\rho\eta}|\leq\Delta_{\dot{\bar{e}}_{i\rho}}=\max\left\{\Delta_{\dot{\bar{e}}_{i\rho r}},\ \Delta_{\dot{\bar{e}}_{i\rho s}}\right\},\\ |e_{i\rho\eta}|\leq\Delta_{\bar{e}_{i\rho}}=|\Delta_{\boldsymbol{s}_i}+\zeta_{iq}-\chi_1\Delta_{\dot{\bar{e}}_{i\rho\eta}}-\beta_1\Delta_{\dot{\bar{e}}_{i\rho\eta}}{}^{q_1/p_1}|,\end{cases} \tag{40}$$

where $\Delta_{\dot{\bar{e}}_{i\rho r}}=(\beta_1^{-1}(\Delta_{\boldsymbol{s}_i}+\zeta_{iq}))^{p_1/q_1}$ and $\Delta_{\dot{\bar{e}}_{i\rho s}}=\chi_1^{-1}(\Delta_{\boldsymbol{s}_i}+\zeta_{iq})$. Moreover, equation (16) has the expression of $\bar{\boldsymbol{e}}_{i\rho}=[\bar{e}_{i\rho1}\ \bar{e}_{i\rho2}]^{\mathrm{T}}=[a_1\dot{e}_{iy}+b_1e_{iy}\ \ f_1e_{iz}]^{\mathrm{T}}$, that is, $\bar{e}_{i\rho2}=f_1e_{iz}$. Then, the normal position error converges to

$$|e_{iz}|\leq\Delta_{e_{iz}}=|f_1|^{-1}|\bar{e}_{i\rho2}|\leq|f_1|^{-1}\Delta_{\bar{e}_{i\rho}}. \tag{41}$$

By using the first item of (16), a first-order system could be established as

$$\dot{e}_{iy}+a_{11}e_{iy}=\zeta_{i3}, \tag{42}$$

where $a_{11}=b_1/a_1$ and $\zeta_{i3}=\bar{e}_{i\rho1}/a_1$ with its bound $|\zeta_{i3}|\leq\zeta_{ir}=\Delta_{\bar{e}_{i\rho}}/|a_1|$. It can be concluded that the first-order system (42) is stable when $a_{11}=b_1/a_1>0$ holds [14]. Likewise, if $a_{11}-\zeta_{i3}e_{iy}^{-1}>0$ or $1-\zeta_{i3}\dot{e}_{iy}^{-1}>0$ holds, the along-track states converge to the bounded regions as

$$\begin{cases}|e_{iy}|\leq\Delta_{e_{iy}}=a_{11}\zeta_{ir},\\ |\dot{e}_{iy}|\leq\Delta_{\dot{e}_{iy}}=\zeta_{ir}.\end{cases} \tag{43}$$

Integrating the along-track dynamics $\ddot{e}_{iy}=-2n_0\dot{e}_{ix}+d_{iy}$ yields $\dot{e}_{iy}(t)=-2n_0e_{ix}(t)+2n_0e_{ix}(0)+\dot{e}_{iy}(0)+\zeta_{i4}=-2n_0e_{ix}(t)+\zeta_{i4}$, where $\zeta_{i4}(t)=\int_0^{t_{if}}[d_{iy}(\tau)]d\tau$ is bounded by $|\zeta_{i4}(t)|\leq\zeta_{is}$. Then, the radial relative position error can be expressed as

$$|e_{ix}|\leq\Delta_{e_{ix}}=(2n_0)^{-1}(\Delta_{\dot{e}_{iy}}+\zeta_{is}). \tag{44}$$

Equations (41)-(44) demonstrate that the parameters in $\boldsymbol{P}_{11}$ affect the coupling relationship between the system states and determine the stable hovering accuracy of the system. In this sense, the non-preset parameter controller designed in this brief can guarantee robustness for the system against unmatched disturbances. Here Theorem 2 is proved. □

Remark 4: To weaken the chattering induced by the sign function in (23), a common way is to replace the sign function $\mathrm{sgn}(\cdot)$ with the following saturation function $\mathrm{sat}(\cdot)$.

$$\mathrm{sat}(s_{i\eta})=\begin{cases}\mathrm{sgn}(s_{i\eta}),&|s_{i\eta}|\geq\epsilon_\eta,\\ s_{i\eta}/\epsilon_\eta,&|s_{i\eta}|<\epsilon_\eta,\end{cases}\quad\eta=1,\ 2 \tag{45}$$

where $\epsilon_\eta>0$ indicates the width of the boundary layer and is a very tiny constant. A minor boundary layer can improve the control accuracy but cause the chattering phenomenon [14]. Thus, a proper boundary layer can eliminate the chattering while keeping the state error within the allowed range.

Remark 5: In the application of spacecraft formation flying, the value of k_2 is normally one-thousandth of that of k_1. In this sense, there must be $l_1^{-1}\Delta_{im}<\left(k_2^{-1}\Delta_{im}\right)^{1/\gamma_1}$, that is, the system trajectory converges to the bounded region $\Delta_{\boldsymbol{s}_i}=l_1^{-1}\Delta_{im}$, indicating that the synchronization control determines the stable hovering accuracy of the system errors but does not affect the convergence of the system.

Remark 6: Suggestions on parameter selection in $\boldsymbol{P}_{11}$: a_1 and b_1 can be regarded as the coupling gains of e_{iy} and $\dot{e}_{iy}$ entering the radial channel. In view of (20), if $\boldsymbol{P}_{11}\boldsymbol{A}_{12}=\boldsymbol{I}_{2\times2}$ holds, the canonical transformation can ensure the coupled dynamics form of the along-track states. Hence, b_1 and f_1 can be set close to $-(2n_0)^{-1}$ and 1, respectively. In the first-order system (42), $a_{11}=b_1a_1>0$ yields a_1 as a negative number. Generally, the stable hovering accuracy of the relative velocity is about one-thousandth of that of the relative position. In this sense, $a_1\approx10^{-3}b_1\approx-0.4$. In addition, it is easy to deduce that the matrix $\boldsymbol{S}$ in (20) is nonsingular when these parameters are select above.

IV. Numerical Simulations

To testify the above theoretical analysis, the spacecraft formation hovering without along-track thrust is simulated. The formation system consists of a virtual leader and three followers who communicate with each other. The orbital elements of the leader in a circular orbit are listed in Table I. In this brief, the nonlinear J_2 perturbation and atmospheric drag in [28] are employed here, and detailed derivations are not repeated for brevity. Meanwhile, the linear quadratic regulator (LQR) and the non-singular terminal sliding mode controller (NTSMC) are used in comparative experiments, and the detailed derivation and parameter setting for both controllers can be referred to [13].

Fig. 2 depicts the feasible set of initial positions (8). As can be seen, changing the range of y will generate different feasible sets. Then, the initial and desired states of followers in Table II are set by using the linear set (10), where $n_0 \approx 1.1 \times 10^{-3}$ rad/s. The control parameters are chosen as: $\alpha_1 = 3 \times 10^{-3}$, $\chi_1 = \beta_1 = 0.5$, $q_1 = 11$, $p_1 = 9$, $k_1 = 3 \times 10^{-3}$, $k_2 = 1 \times 10^{-6}$, $a_1 = -0.4$, $b_1 = -454.5$, $f_1 = 1$, $k_3 = 3 \times 10^{-5}$, $\kappa_{11} = 20$, $\kappa_{12} = 850$, $\kappa_{13} = 950$, and $\kappa_{14} = 0.4$.

TABLE I
Orbital Elements of the Leader.

Orbit elements	Value	Unit
Semi-major axis	6878000	m
Eccentricity	0	-
Inclination	42	deg
Right ascension of ascending node	-60	deg
Argument of latitude	30	deg

TABLE II
Initial and Desired States of Followers.

State	Followers		
	Follower 1	Follower 2	Follower 3
$\boldsymbol{v}_{ig}$ (m/s)	$[0,\ 200n_0,\ 0]^{\mathrm{T}}$	$[0,\ 200n_0,\ 0]^{\mathrm{T}}$	$[0,\ 200n_0,\ 0]^{\mathrm{T}}$
$\boldsymbol{\rho}_{ig}$ (m)	$[1100,\ 400,\ 500]^{\mathrm{T}}$	$[1200,\ 380,\ 450]^{\mathrm{T}}$	$[1300,\ 360,\ 400]^{\mathrm{T}}$
$\boldsymbol{\rho}_{id}$ (m)	$[1200,\ 0,\ 0]^{\mathrm{T}}$	$[1300,\ 0,\ 0]^{\mathrm{T}}$	$[1400,\ 0,\ 0]^{\mathrm{T}}$

Fig. 3 presents the hovering trajectories of three followers under the action of SC (23). Every follower synchronously flies from the initial position f_i^o $(i = 1, 2, 3)$ to the desired hovering position f_i^*. Taking follower 1 as an example, where one orbital period is denoted as $2\pi/n_0 \approx 5712$ s and the final time t_{if} is set to 2.5 orbital periods. Figs. 4 and 5 depict the time histories of the relative position errors and the relative velocity errors, respectively. As can be seen, follower 1 flies to the desired hovering position f_1^* after about one period. Fig. 6 presents the time histories of control inputs. In particular, continuous thrust is required to ensure that the follower 1 hovers in the desired position.

Table III shows the quantitative results of the controllers. The term t_{is} represents the settling time when the position error $\|\boldsymbol{e}_{i\rho}\| = (e_{ix}^2 + e_{iy}^2 + e_{iz}^2)^{1/2}$ of the ith follower reaches and maintains within 5 m, $t_d = \max|t_{is} - t_{js}|$ $(j = 1, 2, 3, i \neq j)$ is defined as the difference between the maximum settling time and the minimum one among followers, $d_{ms} = n^{-1}\sum_{i=1}^{n} d_{is}$ and

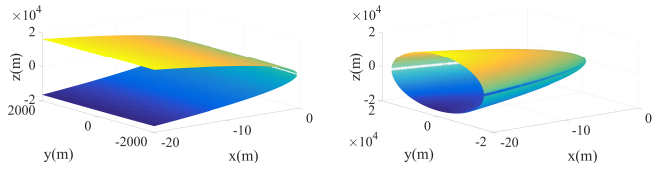

Fig. 2. Feasible sets of initial position when $|y| \leq 2000$m and $|y| \leq 20000$m.

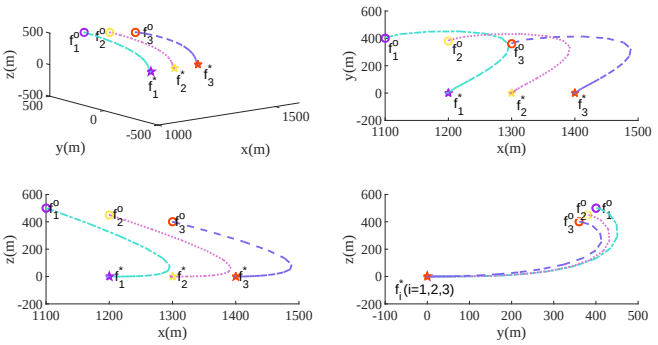

Fig. 3. Hovering trajectories of three followers.

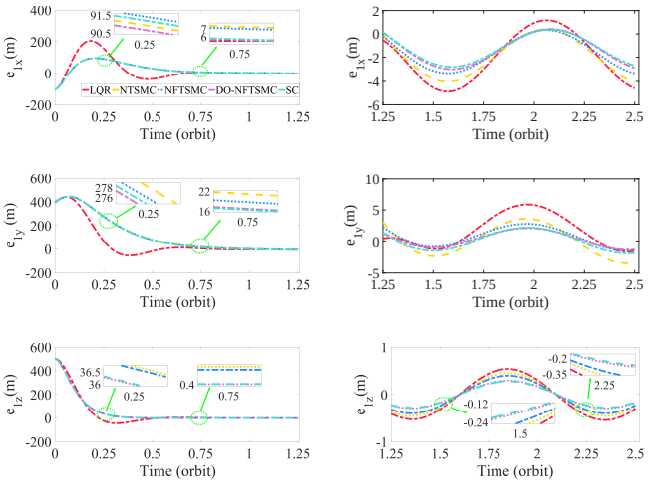

Fig. 4. Relative position error of follower 1.

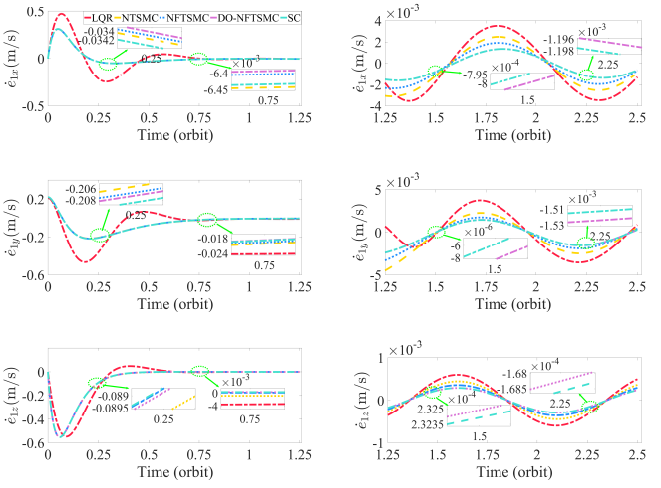

Fig. 5. Relative velocity error of follower 1.

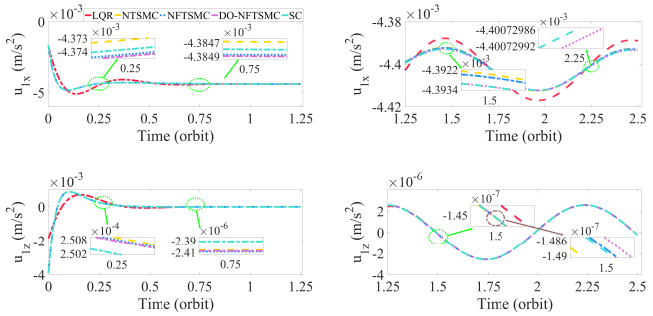

Fig. 6. Underactuated control inputs of follower 1.

TABLE III
PERFORMANCE INDICES OF CONTROLLERS.

Controller	Performance index		
	t_d(orbital period)	$d_{m,s}$(m)	ΔV_m(m/s)
LQR	0.06	3.61	76.19
NTSMC	0.14	3.35	76.36
NFTSMC	0.13	3.31	76.36
DO-NFTSMC	0.17	3.02	76.36
SC	0.02	2.95	76.36

$\Delta V_m = n^{-1}\sum_{i=1}^{n}\int_{t_0}^{t_f}\|\boldsymbol{u}_i\|\mathrm{d}t$ calculate the mean stable error distance and the mean velocity increment for all followers, respectively, where $d_{is} = (t_{if}-t_{is})^{-1}\int_{t_{is}}^{t_{if}}\|\boldsymbol{e}_{i\rho}(t)\|\mathrm{d}t$. Clearly, DO-NTSMC and SC outperform other controllers, especially LQR, in control accuracy. Under the action of SC, the value of the index t_d is the smallest, which is 0.02 orbital period. The results indicate that SC could improve the control accuracy and synchronize the motion between the followers without significantly increasing the velocity increment.

V. CONCLUSION

This brief investigates the feasibility of underactuated spacecraft formation hovering in the case of losing along-track thrust. Based on the nonlinear and linear relative orbital dynamics, the feasible set of initial positions is derived. Moreover, a non-preset parameter underactuated synchronization control scheme is proposed using the inherent coupling of the system state, the finite-time disturbance observer, and the sliding mode technique. The presented controller can effectively eliminate the initial offsets, cope with the influence of unmatched disturbances on the control accuracy, and synchronize every follower motion with that of nearby followers. It is promising to extend the underactuated control scheme to elliptic orbits.

REFERENCES

[1] C. Han, S. Bai, X. Sun and Y. Rao, "Hovering formation control based on two-stage constant thrust," *J. Guid. Control Dyn.*, vol. 43, no. 5, pp. 1–14, 2019.

[2] L. Zhang and P. Q. Ge, "High precision dynamic model and control considering J2 perturbation for spacecraft hovering in low orbit," *Adv. Space Res.*, vol. 67, no. 7, pp. 2185–2198, 2021.

[3] L. A. Sobiesiak and C. J. Damaren, "Lorentz-Augmented Spacecraft Formation Reconfiguration," *IEEE Trans. Control Syst. Technol.*, vol. 24, no. 10, pp. 514–524, 2015.

[4] X. Bai, Y. He and X. Ming, "Low-thrust reconfiguration strategy and optimization for formation flying using jordan normal form," *IEEE Trans. Aerosp. Electron. Syst.*, vol. 57, no. 5, pp. 3279–3295, 2021.

[5] D. Arnas and R. Linares, "Uniform Satellite Constellation Reconfiguration," *J. Guid. Control Dyn.*, vol. 45, no. 7, pp. 1241–1254, 2022.

[6] Y. L. Zhang, X. Y. Zeng and F. D. Zhang, "Spacecraft hovering flight in a binary asteroid system by using fuzzy logic control," *IEEE Trans. Aerosp. Electron. Syst.*, vol. 55, no. 6, pp. 3246–3258, 2019.

[7] W. Wang, D. Wu, G. Mengali and A. Alessandro, "Asteroid hovering missions from a fuel-consumption viewpoint," *J. Guid. Control Dyn.*, vol. 43, no. 7, pp. 1374–1382, 2020.

[8] Z. Dang, Z. Wang and Y. Zhang, "Modeling and analysis of relative hovering control for spacecraft," *J. Guid. Control Dyn.*, vol. 37 no. 4, pp. 1091–1102, 2014.

[9] S. J. Bai, C. Han and X. C. Sun, "Teardrop hovering formation for elliptical orbit considering J2 perturbation," *Aerosp. Sci. Technol.*, vol. 16, pp. 1091–1102, 2020.

[10] T. Chen, J. J. Shan and H. Wen, "Distributed adaptive attitude control for networked underactuated flexible spacecraft," *IEEE Trans. Aerosp. Electron. Syst.*, vol. 55, no. 1, pp. 215–225, 2019.

[11] Godard, K. D. Kumar and A. M. Zou , "Robust station keeping and reconfiguration of underactuated spacecraft formations," *Acta Astronaut.*, vol. 105, pp. 495–510, 2014.

[12] X. Huang, Y. Yan and Y. Zhou, "Underactuated spacecraft formation reconfiguration with collision avoidance," *Acta Astronaut.*, vol. 131, pp. 166–181, 2017.

[13] X. Huang, Y. Yan and Y. Zhou, "Nonlinear control of underactuated spacecraft hovering," *J. Guid. Control Dyn.*, vol. 39 no. 3, pp. 1–10, 2015.

[14] X. Huang and Y. Yan, "Saturated backstepping control of underactuated spacecraft hovering for formation flights," *IEEE Trans. Aerosp. Electron. Syst.*, vol. 53 pp. 4, pp. 1988–2000, 2017.

[15] X. Huang and Y. Yan, "Output feedback control of underactuated spacecraft hovering in circular orbit with radial or in-track controller failure," *IEEE Trans. Ind. Electron.*, vol. 63 no. 9, pp. 5569–5581, 2016.

[16] D. Ye , A. M. Zou and Z. W. Sun, "Predefined-time predefined-bounded attitude tracking control for rigid spacecraft," *IEEE Trans. Aerosp. Electron. Syst.*, vol. 58, no. 1, pp. 464–472, 2021.

[17] Y. Xiao, A. H. de Ruiter, D. Ye and Z. W. Sun, "Attitude coordination control for flexible spacecraft formation flying with guaranteed performance bounds," *IEEE Trans. Aerosp. Electron. Syst.*, 2022, in press.

[18] H. Z. Zhang, D. Ye, Y. Xiao and Z. W. Sun, "Adaptive control on SE(3) for spacecraft pose tracking with harmonic disturbance and input saturation," *IEEE Trans. Aerosp. Electron. Syst.*, vol. 58, no. 5, pp. 4578–4594, 2022.

[19] D. Sun, C. Wang and W. Shang, "A synchronization approach to trajectory tracking of multiple mobile robots while maintaining time-varying formations," *IEEE Trans. Robot.*, vol. 25 no. 5, pp. 1074–1086, 2009.

[20] Z. Liu, W. D. Chen, J. G. Lu, H. S. Wang and J. C. Wang, "Formation control of mobile robots using distributed controller with sampled-data and communication delays," *IEEE Trans. Control Syst. Technol.*, vol. 24, no. 6, pp. 2125–2132, 2016.

[21] H. T. Yu, H. B. Gao, H. C. Deng and S. Yuan, "Synchronization control with adaptive friction compensation of treadmill-based testing apparatus for wheeled planetary rover," *IEEE Trans. Ind. Electron.*, vol. 69 no. 1, pp. 592–603, 2022.

[22] A. P. Wang, B. X. Mu and Y. Shi, "Event-triggered consensus control for multiagent systems with time-varying communication and event-detecting delays" *IEEE Trans. Control Syst. Technol.*, vol. 27, no. 2, pp. 507–515, 2019.

[23] W. H. Clohessy and R. S. Wiltshire, "Terminal guidance system for satellite rendezvous" *J. Aerosp. Sci.*, vol.9, no.27. pp. 653–674, 1960.

[24] D. J. Zhao and D. G. Yang, "Model-free control of quad-rotor vehicle via finite-time convergent extended state observer," *Int. J. Control Autom. Syst.*, vol. 14, no. 1, pp. 242–254, 2016.

[25] Y. X. Shi and Q. L. Hu, "Observer-based spacecraft formation coordinated control via a unified event-triggered communication," *IEEE Trans. Aerosp. Electron. Syst.*, vol. 57, no. 5, pp. 3307–3319, 2021.

[26] N. Zhou, Y. Q. Xia, M.L. Wang and M.Y. Fu, "Finite-time attitude control of multiple rigid spacecraft using terminal sliding mode," *Int. J. Robust Nonlin. Control*, vol. 25, no. 12, pp. 1862–1876, 2015.

[27] Q. F. Chen, S. M. Veres, Y. N. Wang and Y. H. Meng. "Virtual spring-damper mesh-based formation control for spacecraft swarms in potential fields," *J. Guid. Control Dyn.*, vol. 38, no. 3, pp. 539–546, 2015.

[28] D. Mishne, "Formation control of satellites subject to drag variations and J2 perturbations," *J. Guid. Control Dyn.*, vol. 27, no. 4, pp. 685–692, 2004.